特色专题

基于扫描微探针技术的现代腐蚀电化学研究进展

曹发和[1], 李鑫冉[1], 黄秋雨[1], 肖煜华[1], 张勤号[2]

摘要 基于混合电位理论的经典腐蚀电化学对于腐蚀与防护的研究具有重要的促进作用,但也必须认识到腐蚀反应的多反应耦合非平衡不可逆的特征,并由此导致的 Butler−Volmer 和 Nernst−Planck 方程的过度简化,以及对构成腐蚀的电极反应研究的弱化。从腐蚀方程出发,指出腐蚀电化学的内涵,综述了扫描电化学显微镜(SECM)、扫描振动电极(SVET)、局部电化学阻抗(LEUS)和扫描电化学池显微镜(SECCM)4 种典型扫描探针技术在腐蚀反应动力学、空间物种监测、腐蚀活性分布等方面应用的优势与进展,发现高分辨扫描探针技术可识别低至几个纳米腐蚀点与皮安级腐蚀电流,实现了腐蚀发生发展过程反应活性空间差异与动力学的原位监测,进一步结合计算模拟可量化比较分析腐蚀数据。最后展望了现代腐蚀电化学的发展趋势,可继续从多反应耦合的非平衡不可逆腐蚀反应的本质出发,深度融合跨尺度表征,建立宏观–微观的辩证统一关系。

关键词 腐蚀电化学;多反应;非平衡;扫描探针技术;腐蚀反应动力学

金属材料在服役过程中通常由于环境的作用,发生电化学/化学反应导致性能衰变的过程称之为腐蚀[1−2]。多数金属腐蚀现象都具有电化学特征,即金属及其合金在发生腐蚀时至少有 2 类反应:一类是金属阳极溶解形成离子并释放电子;另一类是阴极去极化反应获得电子过程,如析氢反应和/或吸氧反应[3]。在过去的 40 多年里,包括电化学阻抗谱、极化曲线和电化学噪声在内的多种电化学方法得到快速发展,为腐蚀检测、速率评价、寿命评估和腐蚀机制研究提供了大量且重要的信息。需要指出的是,传统腐蚀电化学的研究对象是平板电极(planar electrode,以一维线性传质模型为基础,一般腐蚀研究电极面积约 1.0 cm^2),所获得的电化学信息是整个电极的平均信息,特别是极化曲线技术,且极化曲线难以获得构成腐蚀的电极反应动力学信息。电化学阻抗谱虽有较宽的频率范围(通常为 10^5~10^{-2} Hz),具有一定程度的时间尺度分辨,但是所获得的界面行为和电荷转移电阻等仍是以整个电极平均信息为基础的结果。电化学噪声方法虽能较好地检测局部腐蚀的发生发展,其不足之处主要是复杂的数据处理和分析方法,以及噪声信号特征与腐蚀信息之间对应关系的建立,一般需要辅以形貌观察等离线物理表征[4−6]。必须指出的是:腐蚀电化学过程包含至少 2 个电化学反应耦合的非平衡电化学过程,并通常伴随化学反应[7],即腐蚀反应具有非平衡不可逆多反应耦合的特点,较大程度上限制了电化学测试技术的应用,也限制了腐蚀电化学的研究与发展。

1. 中山大学材料学院,深圳 518107
2. 宁波大学机械工程与力学学院,宁波 315211

收稿日期:2024−12−16;修回日期:2025−05−06
基金项目:国家自然科学基金项目(52371088, 52071347, 51771174, 51171172, 52201096, 52401132);广东省基础与应用基础研究基金项目(2025A1515012093)
作者简介:曹发和,教授,研究方向为腐蚀电化学基础与应用,电子信箱:caofh5@mail.sysu.edu.cn
引用格式:曹发和, 李鑫冉, 黄秋雨, 等. 基于扫描微探针技术的现代腐蚀电化学研究进展[J]. 科技导报, 2025, 43(17): 49−61; doi:10.3981/j.issn.1000-7857.2024.12.01748

目前对于腐蚀电化学的核心基础理论框架仍是基于混合电位理论(mixed potential theory),获得如下腐蚀方程

$$i = i_{corr}(e^{-\frac{\eta}{\beta_c}} - e^{\frac{\eta}{\beta_a}}) \quad (1)$$

腐蚀电化学的数据分析基本都是建立在该方程的基础上,获得诸如极化电阻(R_p)、阴阳极 Tafel 斜率(β_a 和 β_c)、自腐蚀电流(i_{corr})、自腐蚀电位(E_{corr})、电荷转移电阻(R_{ct})、双电层电容(C_{dl})、膜电阻(R_{film})和扩散阻抗(W)等系列电化学特征参数,这些参数与腐蚀速率及腐蚀机制等存在或紧密或松散的联系。腐蚀电化学方法可通过精准解析界面过程(EIS)、快速量化腐蚀速率(极化曲线)和动态捕捉局部失效(电化学噪声),为工程材料防护、寿命预测及失效分析提供核心技术支持。其优势在于高灵敏度、多尺度覆盖(微观–宏观)及实时监测能力,是工业防腐优化与智能运维的关键工具。很多研究工作围绕不同环境体系、不同金属/涂镀层下实现电化学测试,并试图建立相关电化学特征参数与腐蚀行为之间的联系[8−10]。然而,当前腐蚀电化学常常会遇到困难,如 Tafel 极化线性区不明显,导致线性拟合时偶然性和误差较大;弱极化区阴极和阳极反应的耦合电流难以分离,很难获得具体腐蚀阴阳极反应动力学数据;EIS 分析过度依赖等效电路,但是等效电路自身的物理化学图像不够清晰;对于部分腐蚀体系(如高阻体系、易钝化体系),极化曲线和电化学阻抗谱重复性欠佳等。这些问题的存在易导致对腐蚀电化学数据分析流于形式,使得腐蚀电化学变成测试工具,限制腐蚀电化学的发展。产生这些问题的根源有 2 点。(1) 金属腐蚀多以局部腐蚀形式发生发展(微纳尺度),特别是在腐蚀初期。而电化学阻抗谱和极化曲线测试与分析是以整个测试电极(厘米尺度)的信息为基础,不具备空间分辨。这也是一定程度上腐蚀电化学测试结果重现性欠佳,以及测试结果与电极面积有关的原因。(2) 腐蚀电化学分析基础是基于混合电位理论的腐蚀基本方程,不是各自电化学反应本身,即反应信息不够明确。腐蚀基本方程是对腐蚀电化学阴阳极反应的多步假设和简化而得,而现状是直接应用腐蚀基本方程去分析腐蚀电化学数据,获得相关特征参数,鲜有探讨是否可行及其合理性的工作报道。因此,有必要基于现代电化学和仪器科学的发展,深入微纳尺度,原位实时研究腐蚀基本过程和行为特征,发展现代腐蚀电化学,这将是腐蚀方法研究第 2 次重大机遇与挑战。目前,国内外已开展基于扫描微探针技术的腐蚀行为与动力学研究,并取得了进展。

1 基于扫描探针技术的腐蚀电化学进展

1.1 扫描电化学显微镜(SECM)

1989 年,Bard 等[11−12]引入 SECM 扫描探针技术,并对其操作原理与应用发展做出系列开创性工作。SECM 典型测试原理见图 1,通常具有高传质速率的微/纳米探针在腐蚀金属上方几纳米至几十微米区间三维扫描,使得探针和基底样品电极扩散层相互作用,进而实时收集反应产物或监测局域化学环境变化。依据操作模式与目的不同,双恒电位仪可独立对探针和基底电极施加外部极化,实现对液相体系中腐蚀样品的原位电化学/化学成像,具有微/纳级高空间分辨率、化学灵敏性高与非侵入性特点。SECM 空间分辨率高度依赖于探针几何尺寸和探针/基底电极距离,其中几何尺寸包括电极大小和电极半径与绝缘包裹层半径比值(RG 值)。一般来说,电极尺寸和 RG 值越小,探针可以逼近到基底上方更近距离,分辨率越高。然而,纳米探针制备重复性差,存在热漂移、电化学与静电损伤、精确针尖定位和针尖污染等因素,限制了纳米级高分辨成像[12−13],因此,SECM 应用的常见空间尺寸在微米量级。据报道,SECM 探针直径也可低至约 6 nm,实现 10 nm Au 颗粒上皮安级反应电流的超高分辨成像[14]。

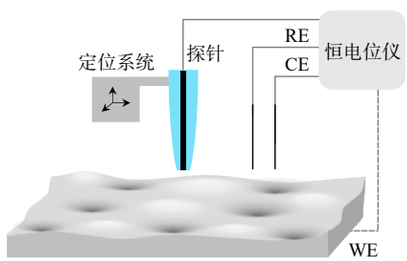

RE 为参比电极,CE 为辅助电极,WE 为工作电极

图 1 SECM 测试原理示意

金属微区腐蚀研究常采用的 SECM 操作模式如图 2 所示。该领域往往基于直流 SECM(DC−SECM)的反馈模式(图 2(a))、产生−收集模式(图 2(b))和氧

化还原竞争模式(图 2(c)),评估腐蚀样品局域电子转移特性[15−17],收集阴阳极反应腐蚀产物(如 Fe^{2+}、O_2、H_2)[18−21],或反应中间物种(如 Mg^+、Cu^+、$Ti^{x\leqslant 3+}$、H_2O_2)[22−26]等。还可通过电位模式(图 2(d)),利用离子选择性探针在无电流扰动下实时监测金属离子(如 Al^{3+}、Mg^{2+}、Zn^{2+}、Na^+、Cl^-)与 pH 演变[27−33]等。亦可采用交流 SECM(AC−SECM,图 2(e))通过向探针施加定频正弦波扰动,在低电导率或无氧化还原媒介液相中,可视化腐蚀样品局域双电层电容与电荷转移电阻等阻抗参数[34−35]。经过 30 余年的发展,SECM 已被广泛应用于裸金属与覆膜金属[13,36−37]、合金与电偶对[35,38],及涂层与缓蚀剂保护下金属[39−40]的局部腐蚀行为与动力学研究。特别是结合 COMSOL 多物理场模拟可进一步获取腐蚀物种空间浓度分布、腐蚀速率、腐蚀反应本征动力学参数,以及绘制腐蚀区域几何形貌等定量腐蚀信息[41−45]。

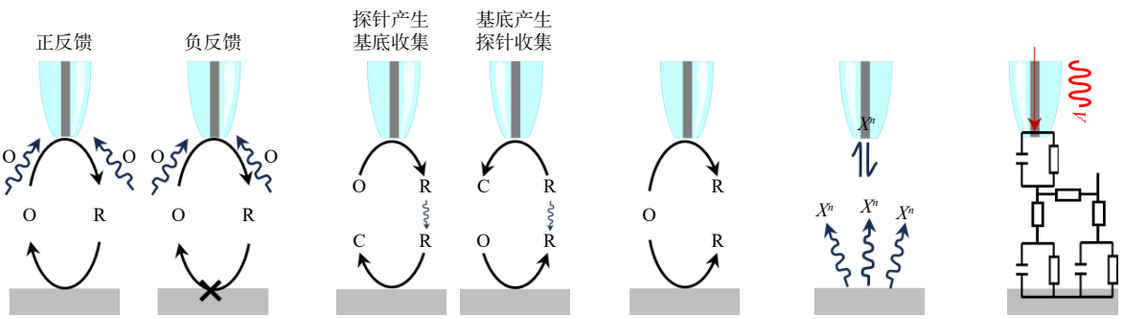

图 2 SECM 操作模式示意

局部腐蚀活性可视化与腐蚀机理分析为 SECM 腐蚀应用的热点研究领域。Li 等[46]采用 SECM 基底产生−探针收集模式,以 I^{3-}/I^-为氧化还原媒介研究了组分及其占比对马氏体不锈钢腐蚀行为的影响,证明了点蚀的萌生与扩展发生在富含 MnS 和 TiN 夹杂相的特定区域。Wang 等[29]成功制备了 5 μm 直径的长效、高选择性 Pt/RuO_x 全固态微型 pH 传感器,在模拟海水中监测了 X80 管线钢预制切口处 pH 随腐蚀进程的演变,发现切口附近首先出现显著 pH 碱化之后逐渐酸化,结合其他物性表征提出了切口处 Fe 溶出 Fe^{2+}后逐渐转换为稳定 α−FeOOH 的反应机制。在异种金属电偶研究中,Alvarez−Pampliega 等[30]采用钨 pH 电极研究了 Fe/Cu 电偶腐蚀过程局域 pH 分布,结果表明 Fe 上酸性与碱性位点共存,揭示了电偶效应驱动下 Fe 表面仅有部分充当阳极。Sundaresan 等[13]基于反馈模式监测了酸性氟化物溶液中钛/不锈钢(TA1/304SS)电偶腐蚀活性位点,证明了电偶对随时间演变的阴阳极极性反转现象。此外,Yanagisawa 等[47]利用 SECM 进行了同种金属异质性微电偶,监测到双相钢马氏体相钝化膜比铁素体相钝化膜具有更好的电子导电性和弱钝化性。在防腐涂层/缓蚀剂评价中,Feng 等[48]在纯锌上制备了三价铬转化膜,通过反馈模式原位研究了转化膜初期局部腐蚀与自愈行为,表明浸泡 24 h 后转化膜开裂发生局部腐蚀,添加聚苯胺可抑制氧还原反应阻碍腐蚀过程,提高转化膜自愈能力。Wang 等[49]基于 AC−SECM 通过监测阻抗|Z|和相位角变化,分析了含单宁酸的氧化石墨烯−介孔二氧化硅涂层的自愈过程,结果表明 AC−SECM 高度依赖于测试频率,高频(60000 Hz)测试下清晰显示 96 h 后涂层发生愈合。对于应力场作用下的腐蚀行为研究,SECM 也可以用提供局部活性以及腐蚀类型演化等信息。Nazarov 等[50]采用 SECM 方法研究了拉伸应力对 AISI 304 不锈钢钝化击穿的影响,结果表明,由于具有破裂钝化膜的阳极性较强的区域与邻近的阴极表面之间的电偶联,应力部位将发生腐蚀。Chen 等[51]通过 SECM 研究结果表明:随着应变水平的增加,304L 不锈钢的表面反应活性显著增强,且应变诱导的 α′马氏体和剪切带区域具有比基体更高的表面反应活性,更容易发生腐蚀,微观电偶腐蚀的激活导致局部腐蚀速率提高。Huang 等[52]使用 SECM 分析不同弹性应力对 TA2 阳极行为的影响,探讨了应力水平、钝化膜以及晶粒结构等对腐蚀行为的影响。以上典型应用仍是把 SECM 作为腐蚀活性/化学环境成像工具,对腐蚀反应过程物种演变与动力学信息研究仍不足。

基于腐蚀电化学反应的中间物种鉴别与反应动力学分析,是深入理解金属腐蚀行为的基础,也是SECM重要腐蚀应用。Li等[20, 53]采用改进的探针产生−基底收集模式,通过定量收集高纯Fe、Cu、Ti阴极氧还原(ORR)过程中H_2O_2,考察了pH、极化电位、电解质阴离子或氧化膜状态对氧还原活性与选择性的影响。结果表明,不同金属表面ORR均非简单4e⁻还原过程,高pH值和强阴极极化促进4e⁻选择性,覆膜金属Ti表明ORR活性往往小于裸金属且高度依赖表面膜活化程度及阴离子介质。对于阳极溶解过程,Bard等[11]还提出了进一步改进的探针产生−基底收集模式,量化了变价金属Ti在酸性氟化物溶液中表观溶解价态随电位依赖性关系,提出Ti在钝化电位之下表观溶解价态低于三价,即使在强阴极极化区间仍存在钛离子溶出。此外,基底产生−探针收集模式成功用于金属Mg溶解过程Mg^+的监测,为Mg溶解的负差数效应提供了直接电化学证据[22]。关于腐蚀反应动力学研究,其往往基于反馈模式,在含有氧化还原媒介的溶液中测试探针对样品表面逼近曲线,通过理论逼近电流公式拟合测试值已获媒介在金属表面有效再生速率常数,以量化金属腐蚀活性。代表性研究如Asserghine等[54]采用FcMeOH作为媒介研究了其在Ti4G表面的钝化膜再生速率,证明钝化膜浸泡时间延长生成速率减慢,20 min时达到稳定最小值,Ti4G发生完全钝化。然而简化模型可能造成理论量化结果与实际结果偏差。

COMSOL多物理场模拟使SECM数据进入量化新阶段,其不但可以定量氧化还原媒介再生速率[55],还可定量具体腐蚀本征动力学参数[56],或模拟腐蚀物种的三维空间分布与腐蚀几何维度成像[40,43]。Zhang等[57]首次将改性的探针产生−基底收集模拟应用于腐蚀领域,活性金属Fe探针上同时发生析氢与溶解反应,基底电极通过定量高效率(91%)收集探针H_2,成功从Fe表观腐蚀电流中分离出净析氢电流,进一步构建COMSOL二维轴对称模型,基于Butler−Volmer方程和Fick定律模拟出酸性高氯酸钠溶液中Fe表面析氢反应本征速率常数为2.5×10^{-6} cm/s,传递系数为0.7。Clark等[43]将半径700 nm次微米Pt电极用于316L不锈钢点蚀高分辨成像,之后将SECM电化学数据结合三维COMSOL多物理模拟,量化相距1 μm点蚀坑的空间几何维度并报道点蚀动态演化过程。

发展至今,SECM已开发出多种功能型探针,并常采用多模式结合,或与其他扫描探针技术、谱学技术及理论计算结合,在更全面分析和深入认识金属局部腐蚀行为中展现出巨大应用潜力[18,58−60]。典型工作如Zhu等[61]开发了一种全固态Pt−Pt/IrO_x超微电极,用于316L不锈钢在6.0%氯化铁溶液中开路电位下的电化学/化学可视化研究,同时监测局部阳极溶出的Fe^{2+}与局部阴极质子消耗引起的pH变化。扫描清楚地显示了局部阳极电流和阴极pH峰位置之间的表观距离约为84 μm,高度为15 μm。为最小化电场失真,Xavier等[26]开发了三壁超微电极探针,通过引入内置参比电极使参比电极尽可能接近离子选择性电极,实现了AZ63镁合金上方Mg^{2+}、pH的同时监测。Zhang等[57]采用反馈模式、基底产生−探针收集模式,及电位模式SECM,对Ni^{2+}、H^+、H_2监测研究了镍钛诺在NaCl溶液中异质活性与局域pH环境变化,观察到Ni^{2+}溶出阳极区域的局部酸化与阴极区域的碱化。Bastos等[18]和Chen等[51]结合SECM与原位表面增强拉曼光谱、COMSOL模拟、第一性原理计算及分子动力学模拟,深入分析了氧化膜特性对高纯钛析氢及吸氧反应行为与动力学影响。综上,多功能、多模式、多技术结合已然成为SECM在腐蚀领域研究的重要发展方向,但目前仍缺乏从电化学反应角度深入研究腐蚀反应相关研究。

1.2 扫描振动电极(SVET)

20世纪80年代,Jadhav等[62]首次将SVET应用于腐蚀研究。其基本测试原理见图3,其中定频正弦振动的探针(通常垂直振动)位于被测金属上方,样品处于自由腐蚀或极化状态。金属腐蚀诱发局部阴阳极离子流动,形成局部电场,振动探针通过测试样品表面振动幅度内电位差$\triangle V$,进而基于欧姆定律$i=-k\triangle V/\triangle d$($k$为溶液电导率,$d$为2个振动点间距)获取样品上方局部电流密度演变的电化学图像,电流正负可反映局域阴阳极特性。该技术通常采用10~30 μm沉积铂黑的Pt振动电极作为探针,且探针−基底间隔一般大于4倍探针振幅,以防撞击基底、避免探头屏蔽效应或高估真实电流。当探针−基底间距为典型值100 μm时,SVET空间分辨率约为200 μm。SVET对腐蚀点源电压与电流信号的检测还受溶液电导率等

影响,在 0.005~0.5 mol/L NaCl 溶液中其可识别约 200 nV 电压差和低至几个纳安的腐蚀电流[63]。

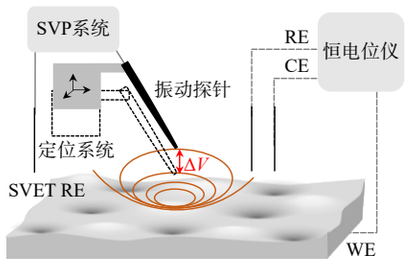

RE 为参比电极,CE 为辅助电极,WE 为工作电极

图 3 SVET 测试原理示意

SVET 可方便识别腐蚀局部阴阳极位置或相对活性,在局部腐蚀(尤其是电偶腐蚀、焊缝腐蚀和应力腐蚀等)[64−67],或防腐涂层与缓蚀剂评价中具有广泛应用[68−72]。Nguyen 等[73]通过 SVET 研究了铈盐对锌基牺牲涂层钢切割边缘的影响,表明铈盐加速了锌基牺牲层的电偶腐蚀,硝酸铈存在下加速尤为严重。此外,铝、镁合金元素的加入促进了局部腐蚀,影响了腐蚀产物的形成和分布。Zhou 等[74]研究了搅拌摩擦焊(FSW)工艺中转速对 AZ31 镁合金焊接接头腐蚀性能的影响,SVET 结果显示在 1800 r/min 下形成的镁合金焊接接头表面电流最小,电流差值约为 0.86 mA/cm^2,远小于其他转速下电流差值(可高达约 12 mA/cm^2)。该结果与接头显微组织及宏观电化学良好吻合,进一步证明了优化旋转速度有助于焊接过程中的高效热机械处理,细化晶粒,从而提高耐腐蚀性。Yang 等[75]成功将 SVET 技术应用于超强不锈钢应力腐蚀研究,考察了不同拉应力和时间周期下裂纹尖端和基体处的电流密度分布,结果显示裂纹尖端的腐蚀电化学活性更高,且电流密度随施加应力与时间增加而增大。在 1500 MPa 应力下浸泡 96 h 裂纹尖端电流密度急速增加至 10.4 μA/cm^2,约为无应力时电流的 3 倍。相似地,Sun 等[76]采用 SVET 研究了预裂纹超高强度不锈钢 $Cr_{12}Ni_5MoCo_{14}$ 在酸性和应力环境下的电化学行为,探讨了活性差异及其可能的原因。Ge 等[77]通过喷涂在 Q235 碳钢表面合成了具有不同孔隙率的 $Co_{21}Fe_{14}Ni_8Cr_{16}Mo_{16}C_{15}B_{10}$ 高熵金属玻璃涂层,之后利用 SVET 评估系列涂层保护下 Q235 碳钢在氯化钠溶液中局部腐蚀活性演变。扫描结果显示低孔隙率涂层表面平均电位差小于 10 μV,具有优异耐腐蚀性;而高孔隙率涂层表面电位差高达几十毫伏并随时间增加而增大,展示出更高腐蚀反应活性,这对应于高孔隙涂层中存在的大量缺陷。Guo 等[66]首次将丹参提取物用作 Q235 钢在 1 mol/L HCl 溶液中的新型缓蚀剂,SVET 监测表明缓蚀剂加入显著延缓了阳极溶解,浸泡 24 h 后最大缓蚀效率达到 91.3%,并在 72 h 内保持在 90.4%。

相较 SECM,SVET 提供振动平面内所有离子电流信息而非与腐蚀过程直接相关的物种浓度,缺乏对离子种类的化学鉴别,与腐蚀反应自身相关性弱;探针的振动及其造成的物种扩散与屏蔽效应,导致样品−探针较大间隔(通常为 100~200 μm),分辨率通常低于 SECM;此外,溶液电导率 k 默认为定值可能对剧烈腐蚀样品产生较大误差[78]。因此,SVET 往往被视为半定量的腐蚀可视化技术,而难以真正确定腐蚀反应及评估腐蚀速率。

基于 COSMOL 模拟,SVET 结果定量及其离子电流测试结果与反应物种的关联成为可能[79−82]。例如,Kozlica 等[64]利用 SVET 测试了 AZ31−AA5083 镁铝合金板电偶腐蚀离子通量分布,通过考虑金属 Mg 和 Al 阴阳极腐蚀反应及其后水解过程,建立了基于 AZ31 镁和 AA5083 铝的铆接板腐蚀演化的 COMSOL 数值模型,成功模拟了电偶腐蚀产物空间分布及其演变,该模型与 SVET 实验阴极阳电流密度分布良好匹配,证明了镁铝双层氢氧化物沉积行为。然而,采用 COMSOL 模拟 SVET 数据需假设可能发生的各类腐蚀反应,以构建合理的腐蚀物理模型,操作的复杂与不确定性使 SVET 定量分析仍较为困难,迄今为止,SVET 腐蚀应用仍集中于局部腐蚀半定量成像研究,难以实现对构成腐蚀的电化学反应和化学反应的定量定性研究。

1.3 局部电化学阻抗谱(LEIS)

20 世纪 90 年代,Lillard 等[83]和 Chang 等[84]提出了另一种扫描探针技术 LEIS,其测试基本原理见图 4。测试过程样品整体被施加定频正弦电压扰动,通过测试探针中双微电极间电压差△V 与微电极间隔求得局部电流,进而结合局部电流与施加扰动电位获取局部阻抗,该阻抗值代表探针/溶液/样品 3 组分界面及其区间内总阻抗[85]。LEIS 测试不依赖于溶液中氧化还原物种的存在,其空间分辨率通常由双微电

极探针尺寸(通常为 Pt 电极)、2 个微电极丝间隔以及探针−基底距离决定。由于探针结构复杂,该技术高空间分辨率有限,最佳分辨率可达约 10 μm[84]。通过与更高分辨的探针装置耦接(如 AFM−LEIS[86]、SECCM−LEIS[87]),可显著提高其分辨率。据报道,采用 SECCM 的准参比电极向基底样品施加交流偏压,SECCM−LEIS 的分辨率可高达 180 nm[88]。

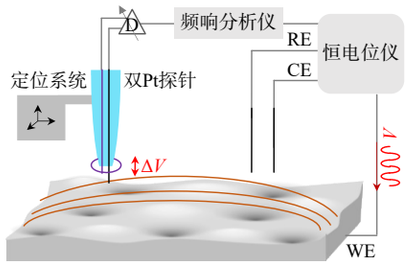

RE 为参比电极,CE 为辅助电极,WE 为工作电极

图 4 LEIS 测试原理示意

基于此,LEIS 与 AC−SECM 均通过正弦扰动测试界面与溶液区阻抗,可在低电导率溶液中进行,便于对腐蚀初期与末期的缓慢反应阶段获得理想电化学成像质量,适用于腐蚀发生发展的完整过程监测与定量分析。相较而言,LEIS 探针双微电极配置导致其空间分辨率通常低于 AC−SECM[89]。目前,LEIS 已被报道用于缓蚀剂、涂层、电偶对与应力作用等腐蚀体系的无损检测[90−94]。Liu 等[92]采用 LEIS 在 10 Hz 下评价了苯并三唑缓蚀剂复合涂层对 Q235 碳钢表面划痕的腐蚀自愈能力。LEIS 结果显示划痕处的阻抗低于周围区域,从腐蚀初期 2 h 至末期 36 h 划痕处局部阻抗增加了 3.1×10^4 Ω,而在无缓蚀剂保护下阻抗值降低了 3.1×10^4 Ω,有力证明了新型缓蚀剂的高效腐蚀抑制效果。Liu 等[93]利用 LEIS 监测了 Ti6Al4V/AA6061 异种金属焊接头在质量百分比为 3.5% NaCl 溶液中长达 16 d 的电偶腐蚀行为,结果显示腐蚀初期接头处腐蚀阻抗最小,随浸泡周期延长腐蚀逐渐扩展到 Al 基体,证明了腐蚀主要发生在铝基体和焊缝处金属,导致点蚀和腐蚀产物的大量积累。Li 等[95]通过 LEIS 技术研究了拉伸应力和压缩应力及力的大小对 X70 管道钢腐蚀的影响。Tang 等[96]则通过 LEIS 清晰地揭示了应力对 X70 管道钢在近中性 pH 条件下阳极溶解行为的影响,并表征了应力、裂纹尖端应力集中效应以及时间因素对局部溶解速率的贡献。Nazarov 等[97]使用 LEIS 研究机械应力对碳钢(SAE 1008)和奥氏体不锈钢(301LN)表面钝化膜的影响,以及这些区域在应力存在下重新钝化的能力。

通常 LEIS 与 AC−SECM 均在固定频率下测试,具有高度频率依赖性,阻抗原始数据解析困难,两者腐蚀应用远低于直流/电位 SECM 与 SEVT 技术。多频响应采集 AC−SECM(4D AC−SECM)的发展弥补了 LEIS 对频率依赖性的不足[33,98]。代表性工作如,Zhu 等[33]采用 4D AC−SECM,对涂漆覆锡低碳钢在 8000~270 Hz 的频率范围内全频阻抗谱进行了自动成像,通过等效电路有效地将整体交流响应分解为与微电极、样品界面电容以及表面局部法拉第过程相关的元件,这些参数具有更清晰的物理意义,而经典 LEIS 技术难以实现。然而全频阻抗谱需要更长测试时间,可能使实时成像结果失真。与 SVET 技术相似,LEIS 也很难建立电化学信息与腐蚀反应之间的直接关联关系,难以据此发展定量的现代腐蚀电化学。

1.4 扫描电化学池显微镜(SECCM)

扫描电化学池显微镜(SECCM)是从微毛细管池技术(microcapillary cell)发展而来,最早的工作可以追溯到 Williams 等[99]在 2009 年提出的利用直径约 1 μm 玻璃管探测电极表面氧化还原活性的扫描微管接触方法(scanning micropipet contact method, SMCM)。2010 年,为了测试局部电化学性质,同时实现表面形貌信息收集,Ebejer 等[100]研究了一种双管 SECCM 方法,该方法通过流经 2 个准参比对电极(QRCE)之间的离子电导电流的交流部分(i_{AC})作为控制探针−基底距离的反馈信号,基本原理如图 5 所示。经过不断发展,SECCM 逐渐成为对各种材料进行微/纳米电化学测量的通用方法,可同时收集电化学和形貌信息数

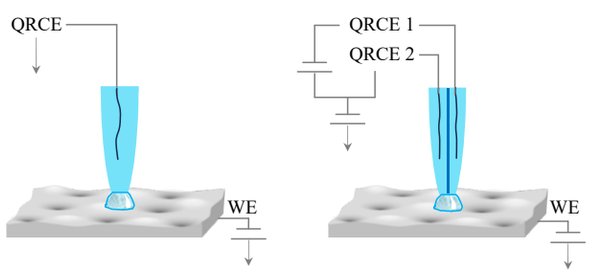

WE 为工作电极

图 5 SECCM 测试原理示意

据,更好地理解微观结构与电化学活性之间的关系。微液滴电解池避免了对邻近区域干扰,借助三维移动装置可获得不同测试条件下的高通量数据。此外,相较其他几项扫描探针技术,SECCM 探针一般为装有测试溶液的纳米级玻璃开口毛细管,其实际分辨率等同于液滴与基底之间的接触尺寸,约为探针直径的 1~1.5 倍,因此 SECCM 具有更高空间分辨率。其分辨率通常为几十纳米,检测电流信号可达皮安级[101]。

由于该方法可以在具有多相结构的材料表面实现原位电化学信息的高分辨成像,自 2019 年起,该方法用于腐蚀研究开始逐渐增多。Yule 等[102-103]利用低碳钢作为研究对象,在低碳钢表面利用 SECCM 技术开展了阴极析氢反应(HER)纳米活性位点分布和晶面对阳极溶剂反应活性差异成像研究。结果表明,酸性溶液内,对于低指数晶面,铁溶解反应以及析氢反应活性均为(100)>(111)>(101),中性溶液内阳极电流则在(101)晶面最大,说明不同晶面的电化学活性存在差异,同时不同溶液条件下晶面的电化学活性差异顺序也会改变。Jayamaha 等[104]则利用 oil-SECCM 技术(在测试基底表面覆盖一层油膜以提高测试液滴稳定性),在 Zn-Al 合金表面实现了高通量微区电化学测试,获得了 6 个具有不同微观结构特征区域的电化学差异。实验结果表明,Zn-Al 合金表面 α 相容易出现早期金属溶解以及氧还原反应,还有金属离子的重新沉积。EDS 结果分析表明这是由于该相处存在高 Al 含量(30%~50%),导致出现 Al 溶解的同时局部 pH 在发生氧还原反应期间升高。截至 2023 年,利用 SECCM 技术研究的金属腐蚀对象包括 Ag[105]、Zn[106]、Cu[107]、Al 合金[108-109]、316L 不锈钢[110],以及 Mg 合金/单晶 Mg[111-112]等。结合其他的形貌表征技术,如背散射电子衍射(EBSD)以及原子力显微镜(AFM),SECCM 技术被广泛地运用于分析阴极和阳极过程的动力学、表面氧化物点蚀以及微结构/组成相关的电化学活性差异。除了电化学活性差异方面的研究,该技术也被用于研究不同晶面取向对缓蚀剂作用效果的影响[113-114]。如 Ebejer 等[100]利用 oil-SECCM 技术发现 Cu 缓蚀剂(BTA-R)在不同晶面上的缓蚀效果存在差距,具体表现在对于 ORR(阴极反应)或者 Cu 溶解反应(阳极反应)抑制效果的差别。

SECCM 在腐蚀研究中具有优越时空分辨率与高通量表征的重要优势,能够在纳米尺度提供腐蚀微区原位的电化学和形貌信息。但其也存在微液滴与 QRCE 稳定性问题,且批量数据处理解读困难,在腐蚀电化学反应机制研究上仍有很大空间。

2 总结与展望

目前,传统以极化曲线和电化学阻抗谱为代表的腐蚀电化学技术,以及与之对应的以腐蚀速率评价与监测为主要目标的腐蚀电化学应用,未能与现代电化学的发展同步。扫描探针技术在腐蚀与防护领域已经开展不少研究,但仍过多关注微区活性,空间分布等作为“显微镜”功能而使用,缺乏从电化学-化学反应角度发展非平衡不可逆的腐蚀电化学。结合课题组的研究以及相关的报道,现代腐蚀电化学可以从以下 3 个方面开展工作。

1)深刻认识多反应耦合的非平衡不可逆腐蚀反应的本质内涵,发展与之适应的电化学测试技术与解析方法,定性定量描述腐蚀反应的构成及其控制因素,发展基于电化学-化学反应的腐蚀电化学。例如,针对不同腐蚀体系特征,联合应用多种扫描探针技术优势,结合 COMSOL 等有限元模拟数据解析方法,建立时空间分辨的“电化学-化学腐蚀”耦合模型,从腐蚀反应出发深入理解腐蚀行为。

2)深度融合原位谱学和量化计算,获得腐蚀反应的物种分子/原子/电子层面信息,深入揭示金属/溶液界面行为,明确腐蚀反应路径与动力学特征,实现多尺度腐蚀行为与机制研究。例如,融合微区实验、分子模拟计算与原位组成表征,探究金属/涂层/溶液界面腐蚀产物与行为演变,指导环境友好型防护技术开发。

3)建立宏观-微观的辩证统一关系,既要发展基于现代扫描微探针的微区技术,实现高时空分辨的腐蚀萌生诱导的研究及其动力学,也要理解宏观尺度下腐蚀发生发展以及腐蚀产物对腐蚀行为影响,且微观要服务于宏观,最终实现腐蚀可控。例如,开展从微观缺陷演化到宏观失效行为的跨尺度研究,结合 SECCM 等高通量测试微区技术与宏观组成、结构及电化学等表征,分析预测不同服役环境金属腐蚀差异,指导高性能合金设计应用。

参考文献(References)

[1] Hou B R, Li X G, Ma X M, et al. The cost of corrosion in China[J]. NPJ Materials Degradation, 2017, 1: 4.

[2] Ma H, Chen X Q, Li R H, et al. First−principles modeling of anisotropic anodic dissolution of metals and alloys in corrosive environments[J]. Acta Materialia, 2017, 130: 137−146.

[3] Davydov A, Rybalka K V, Beketaeva L A, et al. The kinetics of hydrogen evolution and oxygen reduction on Alloy 22[J]. Corrosion Science, 2005, 47(1): 195−215.

[4] Chen A N, Cao F H, Liao X N, et al. Study of pitting corrosion on mild steel during wet–dry cycles by electrochemical noise analysis based on chaos theory[J]. Corrosion Science, 2013, 66: 183−195.

[5] Cao F H, Zhang Z, Su J X, et al. Electrochemical noise analysis of LY12−T3 in EXCO solution by discrete wavelet transform technique[J]. Electrochimica Acta, 2006, 51(7): 1359−1364.

[6] Cottis R. Interpretation of electrochemical noise data[J]. CORROSION, 2001, 57(3): 265−285.

[7] 曹楚南. 腐蚀电化学原理[M]. 3版. 北京: 化学工业出版社, 2020.

[8] Zhang Y X, Zhao M, Zhang J X, et al. Excellent corrosion protection performance of epoxy composite coatings filled with silane functionalized silicon nitride[J]. Journal of Polymer Research, 2018, 25(5): 130.

[9] Tan B C, Zhang S T, Liu H Y, et al. Corrosion inhibition of X65 steel in sulfuric acid by two food flavorants 2–isobutylthiazole and 1−(1, 3−Thiazol−2−yl) ethanone as the green environmental corrosion inhibitors: Combination of experimental and theoretical researches[J]. Journal of Colloid and Interface Science, 2019, 538: 519−529.

[10] Ye Y W, Zou Y J, Jiang Z L, et al. An effective corrosion inhibitor of N doped carbon dots for Q235 steel in 1 M HCl solution[J]. Journal of Alloys and Compounds, 2020, 815: 152338.

[11] Bard A J, Fan F R F, Kwak J, et al. Scanning electrochemical microscopy introduction and principles[J]. Analytical Chemistry, 1989, 61(2): 132−138.

[12] Bard A J , Mirkin M V. Scanning electrochemical microscopy[M]. Boca Raton: CRC Press, 2022.

[13] Sundaresan V, Marchuk K, Yu Y, et al. Visualizing and calculating tip−substrate distance in nanoscale scanning electrochemical microscopy using 3−dimensional super−resolution optical imaging[J]. Analytical Chemistry, 2017, 89: 922−928.

[14] Sun T, Yu Y, Zacher B J, et al. Scanning electrochemical microscopy of individual catalytic nanoparticles[J]. Angewandte Chemie International Edition, 2014, 53(51): 14120−14123.

[15] Yan Z Z, Zhang Q H, Cai H R, et al. Study on the galvanic corrosion of titanium and stainless steel couple with the synergistic effect of proton and fluoride ion[J]. Corrosion Science, 2022, 206: 110541.

[16] Zhou Q X, Wang Y C, Tallman D E, et al. Simulation of SECM approach curves for heterogeneous metal surfaces[J]. Journal of the Electrochemical Society, 2012, 159(7): H644−H649.

[17] Zhu R K, Nowierski C, Ding Z F, et al. Insights into grain structures and their reactivity on grade−2 Ti alloy surfaces by scanning electrochemical microscopy[J]. Chemistry of Materials, 2007, 19(10): 2533−2543.

[18] Bastos A C, Simões A M, González S, et al. Imaging concentration profiles of redox−active species in open−circuit corrosion processes with the scanning electrochemical microscope[J]. Electrochemistry Communications, 2004, 6(11): 1212−1215.

[19] Zhu Z J, Zhang H, Bai Y H, et al. Crevice corrosion behavior of 201 stainless steel in NaCl solutions with different pH values by *in situ* monitoring[J]. Materials, 2024, 17(5): 1158.

[20] Li X R, Meng X Z, Zhang Q H, et al. *In situ* studies of hydrogen evolution kinetics on pure titanium surface: The effects of pre−reduction and dissolved oxygen[J]. The Journal of Physical Chemistry C, 2022, 126(4): 1828−1844.

[21] Asserghine A, Medvidović−Kosanović M, Nagy L, et al. A study of the electrochemical reactivity of titanium under cathodic polarization by means of combined feedback and redox competition modes of scanning electrochemical microscopy[J]. Sensors and Actuators B: Chemical, 2020, 320: 128339.

[22] Zhang Q H, Liu P, Zhu Z J, et al. The study of the H_2O_2 during oxygen reduction process on typically corroding metal surface using tip generation−substrate collection mode of SECM[J]. Corrosion Science, 2020, 164: 108312.

[23] Li X R, Meng X Z, Huang Q Y, et al. Quantitative study on the metal dissolution reaction with multivalent cations by a modified SECM mode: Pure Ti as a case[J]. Corrosion Science, 2024, 235: 112212.

[24] Zhang Q H, Liu P, Zhu Z J, et al. Electrochemical detection of univalent Mg cation: A possible explanation for the negative difference effect during Mg anodic dissolution[J]. Journal of Electroanalytical Chemistry, 2021, 880: 114837.

[25] Zhang Q H, Zhu Z J, Liu P, et al. Corrosion electrochemical kinetic study of copper in acidic solution using scanning electrochemical microscopy[J]. Journal of the Electrochemi-

cal Society, 2019, 166(13): C401−C409.

[26] Xavier J R, Vinodhini S P, Raja Beryl J. RETRACTED: Superior barrier, hydrophobic and mechanical properties of multifunctional nanocomposite coatings on brass in marine environment[J]. Materials Science and Engineering: B, 2022, 278: 115637.

[27] Filotas D, Maria Fernandez−Perez B, Nagy L, et al. Multi−barrel electrodes containing an internal micro−reference for the improved visualization of galvanic corrosion processes in magnesium−based materials using potentiometric scanning electrochemical microscopy[J]. Sensors and Actuators, 2019, 296: 126625.1−126625.10.

[28] da Silva R M P, Izquierdo J, Milagre M X, et al. Development of an Al^{3+} ion−selective microelectrode for the potentiometric microelectrochemical monitoring of corrosion sites on 2098−T351 aluminum alloy surfaces[J]. Electrochimica Acta, 2022, 415: 140260.

[29] Wang J, Zhang Q H, Huang Q Y, et al. *In−situ* pH monitoring of pre−notched X80 pipeline steel using an all−solid−state Pt/RuO_x ultra−micro pH sensor[J]. Sensors and Actuators B: Chemical, 2024, 407: 135484.

[30] Alvarez−Pampliega A, Taryba M G, Van den Bergh K, et al. Study of local Na^+ and Cl^- distributions during the cut−edge corrosion of aluminum rich metal−coated steel by scanning vibrating electrode and micro−potentiometric techniques[J]. Electrochimica Acta, 2013, 102: 319−327.

[31] Bastos A C, Taryba M G, Karavai O V, et al. Micropotentiometric mapping of local distributions of Zn^{2+} relevant to corrosion studies[J]. Electrochemistry communications, 2010, 12(3): 394−397.

[32] Xiao Y H, Huang Q Y, Wang J, et al. *In−situ* fabrication of tungsten oxide film pH micro−sensor and its application on the pH monitoring of Fe−Cu galvanic corrosion[J]. Journal of Electroanalytical Chemistry, 2024, 962: 118259.

[33] Zhu Z J, Liu X Y, Ye Z N, et al. A fabrication of iridium oxide film pH micro−sensor on Pt ultramicroelectrode and its application on *in situ* pH distribution of 316L stainless steel corrosion at open circuit potential[J]. Sensors and Actuators B: Chemical, 2018, 255: 1974−1982.

[34] Pal A, Krishna N G, Ravi Shankar A, et al. Localized surface modification during alternating current scanning electrochemical microscopy: Origin and mechanism[J]. Journal of the Electrochemical Society, 2024, 171(9): 091504.

[35] Bandarenka A S, Eckhard K, Maljusch A, et al. Localized electrochemical impedance spectroscopy: Visualization of spatial distributions of the key parameters describing solid/liquid interfaces[J]. Analytical Chemistry, 2013, 85(4): 2443−2448.

[36] Zhu X J, Xu L J, Wu P G, et al. Failure mode of passive film under electric field and chloride environment in concrete[J]. Construction and Building Materials, 2024, 438: 137080.

[37] Zheng Y Q, Zhang Y, Tian Y Q, et al. Microstructure characteristics and degradation behaviors of medical rare−earth Mg−10.6Gd−0.3Ag−*x*(Y/Zn) alloys *in vitro*[J]. Journal of Alloys and Compounds, 2024, 997: 174967.

[38] Liang J, Liu S Q, Peng Z J, et al. Galvanic corrosion behavior of AZ31 Mg alloy coupled with mild steel: Effect of coatings[J]. Journal of Materials Research and Technology, 2023, 24: 7745−7755.

[39] Zhang W W, Li H J, Liu Y, et al. Stevioside–Zn^{2+} system as an eco−friendly corrosion inhibitor for C1020 carbon steel in hydrochloric acid solution[J]. Colloids and Surfaces A: Physicochemical and Engineering Aspects, 2021, 612: 126010.

[40] Li Z Y, Homborg A, Visser P, et al. Spatiotemporally resolved corrosion protection of AA2024−T3 by a lithium−based conversion layer[J]. Corrosion Science, 2024, 233: 112061.

[41] Egbe O, Morrissey B, Kerton F, et al. Anodic expulsion of Cu nanoparticles from a polycrystalline Cu substrate: A novel corrosion and single entity study approach[J]. Nanoscale, 2025, 17: 10609−10619.

[42] Oltra R, Zimmer A, Sorriano C, et al. Simulation of pH−controlled dissolution of aluminium based on a modified Scanning Electrochemical Microscope experiment to mimic localized trenching on aluminium alloys[J]. Electrochimica Acta, 2011, 56(20): 7038−7044.

[43] Clark C M, Vishnoi P, Swihart M T, et al. The effect of cathodic voltage−controlled electrical stimulation of titanium on the surrounding microenvironment pH: An experimental and computational study[J]. Electrochimica Acta, 2021, 393: 138853.

[44] Ma Q Q, Young J, Gao J N, et al. Nanoscale hydrophobicity and electrochemical mapping provides insights into facet dependent silver nanoparticle dissolution[J]. The Journal of Physical Chemistry Letters, 2023, 14(10): 2665−2673.

[45] Ye Z N, Zhu Z J, Zhang Q H, et al. *In situ* SECM mapping of pitting corrosion in stainless steel using submicron Pt ultramicroelectrode and quantitative spatial resolution analysis[J]. Corrosion Science, 2018, 143: 221−228.

[46] Li G J, Li Z Y, Rahimi E, et al. Pit initiation in quenching and partitioning processed martensitic stainless steels[J]. Electrochimica Acta, 2024, 498: 144646.

[47] Yanagisawa K, Nakanishi T, Hasegawa Y, et al. Passivity of

dual−phase carbon steel with ferrite and martensite phases in pH 8.4 boric acid−borate buffer solution[J]. Journal of The Electrochemical Society, 2015, 162: C322−C326.

[48] Feng J Q, Wang Y B, Lin X L, et al. SECM *in situ* investigation of corrosion and self−healing behavior of trivalent chromium conversion coating on the zinc[J]. Surface and Coatings Technology, 2023, 459: 129411.

[49] Wang W, Wang H L, Zhao J, et al. Self−healing performance and corrosion resistance of graphene oxide–mesoporous silicon layer–nanosphere structure coating under marine alternating hydrostatic pressure[J]. Chemical Engineering Journal, 2019, 361: 792−804.

[50] Nazarov A, Vivier V, Vucko F, et al. Effect of tensile stress on the passivity breakdown and repassivation of AISI 304 stainless steel: A scanning kelvin probe and scanning electrochemical microscopy study[J]. Journal of the Electrochemical Society, 2019, 166(11): C3207−C3219.

[51] Chen X, Gussev M, Balonis M, et al. Emergence of micro−galvanic corrosion in plastically deformed austenitic stainless steels[J]. Materials & Design, 2021, 203: 109614.

[52] Huang Q Y, Li X R, Xiao Y H, et al. Effect of elastic stress on anodic dissolution behavior of TA2[J]. Corrosion Science, 2024, 240: 112506.

[53] Li X R, Meng X Z, Zhang Q H, et al. Insight into oxygen reduction activity and pathway on pure titanium using scanning electrochemical microscopy and theoretical calculations[J]. Journal of Colloid and Interface Science, 2023, 643: 551−562.

[54] Asserghine A, Filotás D, Nagy L, et al. Scanning electrochemical microscopy investigation of the rate of formation of a passivating TiO_2 layer on a Ti G4 dental implant[J]. Electrochemistry Communications, 2017, 83: 33−35.

[55] Zhu R K, Qin Z Q, Noël J J, et al. Analyzing the influence of alloying elements and impurities on the localized reactivity of titanium grade−7 by scanning electrochemical microscopy[J]. Analytical Chemistry, 2008, 80(5): 1437−1447.

[56] Zhang Q H, Li X R, Liu P, et al. Quantitative study of the kinetics of hydrogen evolution reaction on aluminum surface and the influence of chloride ion[J]. International Journal of Hydrogen Energy, 2021, 46(80): 39665−39674.

[57] Zhang Q H, Ye Z N, Zhu Z J, et al. Separation and kinetic study of iron corrosion in acidic solution *via* a modified tip generation/substrate collection mode by SECM[J]. Corrosion Science, 2018, 139: 403−409.

[58] Wang J Y, Xie L, Han L B, et al. *In−situ* probing of electrochemical dissolution and surface properties of chalcopyrite with implications for the dissolution kinetics and passivation mechanism[J]. Journal of Colloid and Interface Science, 2021, 584: 103−113.

[59] Asserghine A, Medvidović−Kosanović M, Stanković A, et al. A scanning electrochemical microscopy characterization of the localized corrosion reactions occurring on nitinol in saline solution after anodic polarization[J]. Sensors and Actuators B: Chemical, 2020, 321: 128610.

[60] Li X R, Zhang Q H, Meng X Z, et al. Effect of pretreatments on the hydrogen evolution kinetics of pure titanium using impedance and SECM technologies[J]. Corrosion Science, 2021, 191: 109726.

[61] Zhu Z J, Zhang Q H, Liu P, et al. Quasi−simultaneous electrochemical/chemical imaging of local Fe^{2+} and pH distributions on 316 L stainless steel surface[J]. Journal of Electroanalytical Chemistry, 2020, 871: 114107.

[62] Jadhav N, Gelling V J. Review: The use of localized electrochemical techniques for corrosion studies[J]. Journal of the Electrochemical Society, 2019, 166(11): C3461−C3476.

[63] Bastos A C, Quevedo M C, Karavai O V, et al. Review: On the application of the scanning vibrating electrode technique (SVET) to corrosion research[J]. Journal of the Electrochemical Society, 2017, 164(14): C973−C990.

[64] Kozlica D K, Hernández−Concepción B, Izquierdo J, et al. In situ, real−time imaging of redox−active species on Al/Cu galvanic couple and corrosion inhibition with 2−mercaptobenzimidazole and octylphosphonic acid[J]. Corrosion Science, 2023, 217: 111114.

[65] Li T T, Shi J X, Li R F, et al. Interfacial microstructure and corrosion behaviors of TC4/DP780 steel joints by laser welding with H62 interlayer[J]. Journal of Materials Research and Technology, 2024, 29: 4470−4479.

[66] Guo H, Wang R, Jiang M H, et al. Cement−mortar lining failure and metal release caused by electrochemical corrosion of ductile iron pipes in drinking water distribution systems[J]. Journal of Environmental Sciences, 2025, 152: 488−502.

[67] Ji Y Y, Guo Y J, Xia Y M, et al. Effect of bending deformation on the corrosion behavior of non−brazed and brazed Al composite[J]. Electrochimica Acta, 2024, 481: 143928.

[68] Li H, Zhang Q H, Meng X Z, et al. Active/passive protection and anti−UV waterborne epoxy coatings based on low defect functionalized PDA−GO−CeO_2 material for excellent corrosion control[J]. Chemical Engineering Journal, 2024, 479: 147859.

[69] Zeng C, Zhou Z Y, Mai W J, et al. Exploration on the corrosion inhibition performance of Salvia miltiorrhiza extract as a green corrosion inhibitor for Q235 steel in HCl environ-

ment[J]. Journal of Materials Research and Technology, 2024, 32: 3857−3870.

[70] Yasakau K A, Kuznetsova A, Maltanava H M, et al. Corrosion protection of zinc by LDH conversion coatings[J]. Corrosion Science, 2024, 229: 111889.

[71] Xie Z H, Zhang W X, Li Y Q, et al. Inhibitor−sandwiched polyelectrolyte film for micro/nanopore sealing to enable corrosion−resistant self−healing capability[J]. ACS Applied Polymer Materials, 2024, 6(7): 4037−4049.

[72] Ye Y W, Yang D P, Chen H, et al. A high−efficiency corrosion inhibitor of N−doped citric acid−based carbon dots for mild steel in hydrochloric acid environment[J]. Journal of Hazardous Materials, 2020, 381: 121019.

[73] Nguyen T T, Akbarzadeh S, Thai T T, et al. Effect of cerium salts on the cut−edge of zinc−based sacrificial coatings: Influence of Al and Mg alloying elements on galvanic corrosion[J]. Journal of Alloys and Compounds, 2024, 981: 173711.

[74] Zhou Z R, Chen S J, Hodgson M, et al. Influence of rotation speed on the corrosion behavior of friction stir welded joints in AZ31 magnesium alloy[J]. Journal of Materials Research and Technology, 2025, 34: 1223−1234.

[75] Yang Y, Cheng Y F. Effect of stress on corrosion at crack tip on pipeline steel in a near−neutral pH solution[J]. Journal of Materials Engineering and Performance, 2016, 25(11): 4988−4995.

[76] Sun M, Xiao K, Dong C F, et al. Effect of stress on electrochemical characteristics of pre−cracked ultrahigh strength stainless steel in acid sodium sulphate solution[J]. Corrosion Science, 2014, 89: 137−145.

[77] Ge Y Y, Cheng J B, Xue L, et al. Pore defect and corrosion behavior of HVAF−sprayed $Co_{21}Fe_{14}Ni_8Cr_{16}Mo_{16}C_{15}B_{10}$ high entropy metallic glass coatings[J]. Corrosion Science, 2025, 242: 112564.

[78] Simões A M, Bastos A C, Ferreira M G, et al. Use of SVET and SECM to study the galvanic corrosion of an iron–zinc cell[J]. Corrosion Science, 2007, 49(2): 726−739.

[79] Thébault F, Vuillemin B, Oltra R, et al. Reliability of numerical models for simulating galvanic corrosion processes[J]. Electrochimica Acta, 2012, 82: 349−355.

[80] Thébault F, Vuillemin B, Oltra R, et al. Protective mechanisms occurring on zinc coated steel cut−edges in immersion conditions[J]. Electrochimica Acta, 2011, 56(24): 8347−8357.

[81] Snihirova D, Höche D, Lamaka S, et al. Galvanic corrosion of Ti_6Al_4V−AA2024 joints in aircraft environment: Modelling and experimental validation[J]. Corrosion Science, 2019, 157: 70−78.

[82] Cross S R, Gollapudi S, Schuh C A. Validated numerical modeling of galvanic corrosion of zinc and aluminum coatings[J]. Corrosion Science, 2014, 88: 226−233.

[83] Lillard R S, Moran P J, Isaacs H S. A novel method for generating quantitative local electrochemical impedance spectroscopy[J]. Journal of The Electrochemical Society, 1992, 139: 1007−1012.

[84] Chang W W, Qian H C, Li Z Y, et al. Application and prospect of localized electrochemical techniques for microbiologically influenced corrosion: A review[J]. Corrosion Science, 2024, 236: 112246.

[85] Frateur I, Huang V M, Orazem M E, et al. Local electrochemical impedance spectroscopy: Considerations about the cell geometry[J]. Electrochimica Acta, 2008, 53(25): 7386−7395.

[86] Gharbi O, Ngo K, Turmine M, et al. Local electrochemical impedance spectroscopy: A window into heterogeneous interfaces[J]. Current Opinion in Electrochemistry, 2020, 20: 1−7.

[87] Wang A C, Jin R, Jiang D C. Integrated scanning electrochemical cell microscopy platform with local electrochemical impedance spectroscopy using a preamplifier[J]. Faraday Discussions, 2025, 257: 182−193.

[88] Cheng L, Jin R, Jiang D C, et al. Scanning electrochemical cell microscopy platform with local electrochemical impedance spectroscopy[J]. Analytical Chemistry, 2021, 93(49): 16401−16408.

[89] Skaanvik S A, Gateman S M. Probing passivity of corroding metals using scanning electrochemical probe microscopy[J]. Electrochemical Science Advances, 2024, 4(5): e2300014.

[90] Chen Y F, Wu Y H, Zhao W J. Constructing PANI@CF hybrids enhanced epoxy coatings with integrated functionalities of interfacial enhancement, erosion wear resistance and anti−corrosion[J]. Chemical Engineering Journal, 2024, 488: 150933.

[91] Xu H, Cao R, Ma X L, et al. Corrosion mechanism of the Ti–6Al–4V/AA6061 dissimilar metal CMT welded joint[J]. Journal of Materials Research and Technology, 2025, 35: 6951−6964.

[92] Liu T, Liu Y, Qu D, et al. Smart self−healing coating based on the covalent organic frameworks (COF LZU−1) for corrosion protection of steel[J]. Colloids and Surfaces A: Physicochemical and Engineering Aspects, 2024, 685: 133246.

[93] Liu T, Liu Y, Qu D, et al. Multifunctional epoxy coatings reinforced with LDHs−modified silica microspheres: Synergistic effects on corrosion resistance, thermal insulation, and

flame retardancy[J]. Colloids and Surfaces A: Physicochemical and Engineering Aspects, 2024, 698: 134578.

[94] Lin Y F, Li Z Y, Wang X Q, et al. Effect of coating damage on the micro area corrosion performance of HDR duplex stainless steel[J]. Coatings, 2024, 14(2): 174.

[95] Li M C, Cheng Y F. Corrosion of the stressed pipe steel in carbonate–bicarbonate solution studied by scanning localized electrochemical impedance spectroscopy[J]. Electrochimica Acta, 2008, 53(6): 2831−2836.

[96] Tang X, Cheng Y F. Micro−electrochemical characterization of the effect of applied stress on local anodic dissolution behavior of pipeline steel under near−neutral pH condition[J]. Electrochimica Acta, 2009, 54(5): 1499−1505.

[97] Nazarov A, Vivier V, Thierry D, et al. Effect of mechanical stress on the properties of steel surfaces: Scanning kelvin probe and local electrochemical impedance study[J]. Journal of the Electrochemical Society, 2017, 164(2): C66−C74.

[98] Eckhard K, Erichsen T, Stratmann M, et al. Frequency−dependent alternating−current scanning electrochemical microscopy (4D AC−SECM) for local visualisation of corrosion sites[J]. Chemistry, 2008, 14(13): 3968−3976.

[99] Williams C G, Edwards M A, Colley A L, et al. Scanning micropipet contact method for high−resolution imaging of electrode surface redox activity[J]. Analytical Chemistry, 2009, 81(7): 2486−2495.

[100] Ebejer N, Schnippering M, Colburn A W, et al. Localized high resolution electrochemistry and multifunctional imaging: Scanning electrochemical cell microscopy[J]. Analytical Chemistry, 2010, 82(22): 9141−9145.

[101] Lai Z G, Liu M, Bi P, et al. Perspectives on corrosion studies using scanning electrochemical cell microscopy: Challenges and opportunities[J]. Analytical Chemistry, 2023, 95(43): 15833−15850.

[102] Yule L C, Shkirskiy V, Aarons J, et al. Nanoscale electrochemical visualization of grain−dependent anodic iron dissolution from low carbon steel[J]. Electrochimica Acta, 2020, 332: 135267.

[103] Yule L C, Bentley C L, West G, et al. Scanning electrochemical cell microscopy: A versatile method for highly localised corrosion related measurements on metal surfaces[J]. Electrochimica Acta, 2019, 298: 80−88.

[104] Jayamaha G, Tegg L, Bentley C L, et al. High throughput correlative electrochemistry−microscopy analysis on a Zn−Al alloy[J]. ACS Physical Chemistry Au, 2024, 4(4): 375−384.

[105] Wang Y F, Li M Y, Gordon E, et al. Nanoscale colocalized electrochemical and structural mapping of metal dissolution reaction[J]. Analytical Chemistry, 2022, 94(25): 9058−9064.

[106] Shkirskiy V, Yule L C, Daviddi E, et al. Nanoscale scanning electrochemical cell microscopy and correlative surface structural analysis to map anodic and cathodic reactions on polycrystalline Zn in acid media[J]. Journal of the Electrochemical Society, 2020, 167(4): 041507.

[107] Daviddi E, Shkirskiy V, Kirkman P M, et al. Nanoscale electrochemistry in a copper/aqueous/oil three−phase system: Surface structure−activity−corrosion potential relationships[J]. Chemical Science, 2020, 12(8): 3055−3069.

[108] Li Y J, Morel A, Gallant D, et al. Correlating corrosion to surface grain orientations of polycrystalline aluminum alloy by scanning electrochemical cell microscopy[J]. ACS Applied Materials & Interfaces, 2022, 14(41): 47230−47236.

[109] Li Y J, Morel A, Gallant D, et al. Oil−immersed scanning micropipette contact method enabling long−term corrosion mapping[J]. Analytical Chemistry, 2020, 92(18): 12415−12422.

[110] Coelho L B, Torres D, Bernal M, et al. Probing the randomness of the local current distributions of 316L stainless steel corrosion in NaCl solution[J]. Corrosion Science, 2023, 217: 111104.

[111] Prabhakaran V, Strange L, Kalsar R, et al. Investigating electrochemical corrosion at Mg alloy−steel joint interface using scanning electrochemical cell impedance microscopy (SECCIM)[J]. Scientific Reports, 2023, 13(1): 13250.

[112] Prabhakaran V, Kalsar R, Strange L, et al. Understanding localized corrosion on metal surfaces using scanning electrochemical cell impedance microscopy (SECCIM)[J]. The Journal of Physical Chemistry C, 2022, 126(30): 12519−12526.

[113] Daviddi E, Shkirskiy V, Kirkman P M, et al. Screening the surface structure−dependent action of a benzotriazole derivative on copper electrochemistry in a triple−phase nanoscale environment[J]. The Journal of Physical Chemistry C, Nanomaterials and Interfaces, 2022, 126(35): 14897−14907.

[114] Sun X Y, Liu S Y, Hu P, et al. Microscale corrosion inhibition behavior of four corrosion inhibitors (BTA, MBI, MBT, and MBO) on archeological silver artifacts based on scanning electrochemical cell microscopy[J]. Analytical Chemistry, 2023, 95(39): 14686−14694.

Research progress in modern corrosion electrochemistry based on scanning probe techniques

CAO Fahe[1], LI Xinran[1], HUANG Qiuyu[1], XIAO Yuhua[1], ZHANG Qinhao[2]

1. School of Material, Sun Yat−sen University, Shenzhen 518107, China

2. Faculty of Mechanical Engineering and Mechanics, Ningbo University, Ningbo 315211, China

Abstract Classical corrosion electrochemistry based on mixed potential theory has played an important role in advancing research on corrosion and protection. However, it is also essential to recognize the multi−reaction coupling, non−equilibrium, and irreversible nature of corrosion processes, which often leads to excessive simplifications in the Butler–Volmer and Nernst–Planck equations and a weakened focus on the individual electrode reactions that constitute corrosion. Starting from the fundamental corrosion equation, this work clarifies the connotation of corrosion electrochemistry and reviews the advantages and recent progress of four representative scanning probe techniques—scanning electrochemical microscopy (SECM), scanning vibrating electrode technique (SVET), localized electrochemical impedance spectroscopy (LEIS), and scanning electrochemical cell microscopy (SECCM)—in probing corrosion reaction kinetics, monitoring spatially distributed species, and mapping corrosion activity. High−resolution scanning probe methods have been shown to detect corrosion sites as small as a few nanometers and corrosion currents at the picoampere level, enabling in−situ monitoring of the spatial heterogeneity and kinetics of corrosion processes. When further combined with computational modeling, these techniques allow for quantitative comparative analysis of corrosion data. Finally, the paper summarizes and discusses future trends in modern corrosion electrochemistry, suggesting that further research should be rooted in the intrinsic nature of multi−reaction−coupled, non−equilibrium, irreversible corrosion processes, deeply integrating multi−scale characterization, and establishing a dialectical unity between macroscopic and microscopic perspectives.

Keywords corrosion electrochemistry; multi−reaction; non−equilibrium; scanning probe technology; corrosion reaction kinetic

（责任编辑　王微）